Capillary Meniscus Interaction between Colloidal Particles Attached to a Liquid–Fluid Interface

P. A. KRALCHEVSKY,* V. N. PAUNOV,* I. B. IVANOV,*,[1] AND K. NAGAYAMA†

*Laboratory of Thermodynamics and Physico-Chemical Hydrodynamics, University of Sofia, Faculty of Chemistry, Sofia 1126, Bulgaria; and †Protein Array Project, ERATO, JRDC, 18-1 Higashiarai, Tsukuba, 305, Japan

Received August 5, 1991; accepted November 14, 1991

General expressions for the energy of capillary meniscus forces acting between particles attached to a liquid–fluid interface are derived. These expressions are specified for the cases of two vertical cylinders and two similar spheres partially immersed in a liquid layer on a horizontal solid substrate. The shape of the meniscus around the particles is determined from the Laplace equation by using the method of the matched asymptotic expansions. The derived asymptotic expressions are valid with a very good accuracy when the contact line radius and the interparticle distance are smaller than 100 μm (liquid–gas interface). The range of validity can be wider for emulsion-type interfaces. The capillary meniscus forces turn out to be attractive and very long-ranged. The results can be important for interpreting the surface coagulation phenomena accompanying flotation processes as well as two-dimensional ordering of colloidal particles and protein molecules.

1. INTRODUCTION

It is known that the deformation of a liquid–fluid interface due to trapped colloidal particles gives rise to capillary forces exerted on the particles. Usually these forces are attractive and lead to the formation of clusters. Such effects are observed and utilized in some extraction and separation flotation processes (1, 2). The surface deformations produced by floating particles were studied experimentally by Hinsch (3) by means of a holographic method. The capillary meniscus forces can be one of the main factors leading to the formation of two-dimensional clusters and ordered structures observed with micron-size particles (4, 5) as well as with protein molecules (6–8).

In spite of the well-established importance of the capillary meniscus forces there are only few theoretical works devoted to them. Nicolson (9) derived an analytical expression for the capillary force between two floating bubbles by using a superposition approximation to solve the Laplace equation. This approximated method was developed and applied by Chan *et al.* (10) to floating spheres and horizontal cylinders. In the latter case the Laplace equation reduces to an ordinary differential equation. The capillary forces in this case were calculated by Gifford and Scriven (11) and by Fortes (12).

In the present study we develop a new approach to the theory of capillary meniscus forces. In the next section a general expression for the interaction energy is formulated. By means of the Green formula the integrals over the meniscus volume and surface are transformed to integrals over the three-phase contact lines. This leads to a considerable simplification of the problem. In sections 3 and 4 analytical expressions for the energy of capillary interaction between two *vertical* cylinders and two spheres protruding from a liquid layer

[1] To whom correspondence should be addressed.

0021-9797/92 $5.00

are derived. Numerical results and a discussion are presented at the end of the paper.

2. GENERAL EQUATIONS

a. Interaction Energy

Let us consider a system of N particles attached to a liquid–fluid interface between Phases I and II (for the sake of simplicity only two particles are depicted in Fig. 1). The particles can be solid, liquid, or bubbles. The interface is supposed to be flat and horizontal far from the particles. We choose the coordinate plane xy to coincide with this horizontal surface.

Let

$$z = \zeta(x, y) \qquad [2.1]$$

be the equation describing the surface of the liquid meniscus formed around the particles. ζ can be both positive and negative depending on the particle weight and contact angle—see Fig. 1. In addition we assume that the system under consideration is situated between the planes $z = z_1$ and $z = z_2$, located in Phases I and II, respectively—see Fig. 1. As shown below, these two planes play an auxiliary role: the final results do not depend on z_1 and z_2 (cf., e.g., Eqs. [3.20] and [3.21] below). That is why the exact location of z_1 and z_2 is not important.

We denote by V_{I} and V_{II} the volumes of the respective phases and by V_K the volume of the K-th particle ($K = 1, 2, \ldots, N$). If $\mathbf{r}_1, \mathbf{r}_2, \ldots,$ $\mathbf{r}_N$ are the position vectors of the mass centers of the particles, the free energy of the system will read

$$W(\mathbf{r}_1, \mathbf{r}_2, \ldots, \mathbf{r}_N) = \sum_{K=1}^{N} m_K g Z_K^{(c)} + \sum_{Y=\mathrm{I,II}} m_Y g Z_Y^{(c)} + \sum_{K=1}^{N} \sum_{Y=\mathrm{I,II}} \omega_{KY} A_{KY} + \gamma \Delta A. \qquad [2.2]$$

Here

$$Z_K^{(c)} = \frac{1}{V_K} \int_{V_K} z dV \quad \text{or}$$

$$Z_Y^{(c)} = \frac{1}{V_Y} \int_{V_Y} z dV \qquad [2.3]$$

is the z coordinate of the mass center of the respective particle or phase, m_K and m_Y are masses, g is the gravity acceleration, A_{KY} and ω_{KY} are the area and the surface free energy density of the interface between Particle K and Phase Y; γ is the interfacial tension of the boundary between Phases I and II, and ΔA is the difference between the areas of the latter boundary and of the portion of the plane xy included in the system. We use ΔA here because it is a finite quantity even if the area of the interface between Phases I and II is infinite. (Note that the free energy W in Eq. [2.2] is defined up to an additive constant.) In fact ω_{KY} represents the density of the surface grand thermodynamical potential; ω_{KY} coincides with the respective interfacial tension when Particle K is fluid and there are no insoluble adsorbed species—see, e.g., (13, 14).

The interaction energy ΔW between particles 1, 2, . . . , N can be defined as

$$\Delta W(\mathbf{r}_1, \mathbf{r}_2, \ldots, \mathbf{r}_N) = W(\mathbf{r}_1, \mathbf{r}_2, \ldots, \mathbf{r}_N) - W_\infty, \qquad [2.4]$$

where W_∞ is the value of W at infinite interparticle separations.

The main problem for calculating the interaction energy ΔW is the determination of

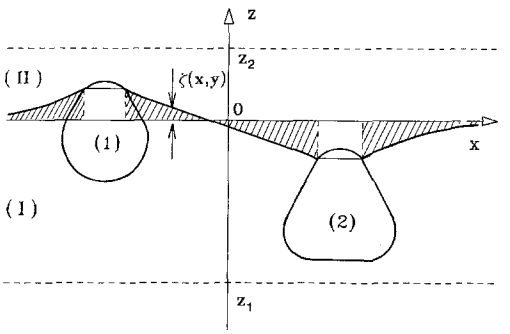

FIG. 1. Sketch of two particles attached at the interface between two fluid phases I and II.

the meniscus profile $\zeta(x, y)$. In general $\zeta(x, y)$ satisfies the Laplace equation of the capillarity (15–17),

$$(1 + \zeta_y^2)\zeta_{xx} - 2\zeta_x\zeta_y\zeta_{xy} + (1 + \zeta_x^2)\zeta_{yy} = q^2\zeta(x, y)(1 + \zeta_x^2 + \zeta_y^2)^{3/2}, \quad [2.5]$$

where

$$\zeta_x \equiv \frac{\partial\zeta}{\partial x}, \qquad \zeta_y \equiv \frac{\partial\zeta}{\partial y}, \qquad \zeta_{xx} \equiv \frac{\partial^2\zeta}{\partial x^2},$$

$$\zeta_{xy} \equiv \frac{\partial^2\zeta}{\partial x\partial y}, \qquad \zeta_{yy} \equiv \frac{\partial^2\zeta}{\partial y^2}$$

$$q^2 = \Delta\rho g/\gamma, \quad \Delta\rho = \rho_{\mathrm{I}} - \rho_{\mathrm{II}}, \quad [2.6]$$

where ρ_{I} and ρ_{II} are the mass densities of Phases I and II. The boundary conditions for Eq. [2.5] are the conditions for mechanical equilibrium at the three-phase contact lines—see, e.g., (18).

Equations [2.2]–[2.6] provide a basis for calculating the capillary interactions in each specified case. As demonstrated below, the problem considerably simplifies when the slope of the meniscus surface $\zeta(x, y)$ is small.

b. Meniscus Surface Energy

Here we consider separately the surface free energy $\gamma\Delta A$ of the boundary between Phases I and II. Eqs. [2.2] and [2.4] imply that the contribution of the meniscus surface free energy into the interaction energy ΔW is

$$\Delta W_{\mathrm{m}} = \gamma(\Delta A - \Delta A_\infty), \quad [2.7]$$

where ΔA_∞ is the value of ΔA at infinite interparticle distances. Let $C_1, C_2, \ldots, C_N$ be the projections of the three-phase contact lines of particles $1, 2, \ldots, N$ on the plane xy—see Fig. 2. We denote by A_K^{c} the area encircled by the contour C_K, and by $A_{K\infty}^{\mathrm{c}}$ the value of A_K^{c} for infinite interparticle distances. Then Eq. [2.7] can be transformed to read

$$\Delta W_{\mathrm{m}} = \gamma[\Delta A^{\mathrm{P}} - \Delta A_\infty^{\mathrm{P}} - \sum_{K=1}^{N}(A_K^{\mathrm{c}} - A_{K\infty}^{\mathrm{c}})], \quad [2.8]$$

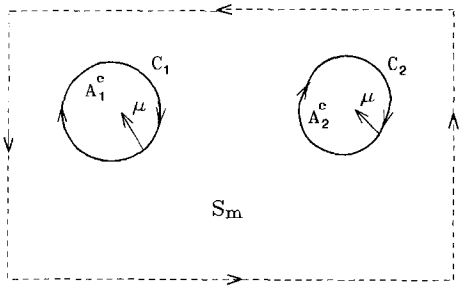

FIG. 2. Sketch of the integration contours in Eq. [2.18]. A_K^{c} is the area encircled by the contour C_K, which represents the projection of the contact line of the ith particle on the plane xy. μ is the running inner unit normal; S_{m} is the area outside the contours C_K.

where ΔA^{P} is the difference between the area of the meniscus surface and the area of its projection on the plane xy. Hence ΔA^{P} can be expressed as follows

$$\Delta A^{\mathrm{P}} = \int_{S_{\mathrm{m}}} \left\{ \left[1 + \left(\frac{\partial\zeta}{\partial x}\right)^2 + \left(\frac{\partial\zeta}{\partial y}\right)^2 \right]^{1/2} - 1 \right\} ds, \quad [2.9]$$

where $ds = dxdy$ is the surface element and the integration is carried out over the projection of the meniscus surface on the plane xy. In fact S_{m} is the surface outside the contours C_K ($K = 1, 2, \ldots, N$)—see Fig. 2. When the slope of the meniscus surface is small, i.e.,

$$\left(\frac{\partial\zeta}{\partial x}\right)^2 \ll 1, \quad \left(\frac{\partial\zeta}{\partial y}\right)^2 \ll 1, \quad [2.10]$$

the square root in Eq. [2.9] can be expanded in series to yield

$$\Delta A^{\mathrm{P}} = \frac{1}{2}\int_{S_{\mathrm{m}}} (\nabla_{\mathrm{II}}\zeta)\cdot(\nabla_{\mathrm{II}}\zeta)ds, \quad [2.11]$$

where

$$\nabla_{\mathrm{II}}\zeta = \left(\frac{\partial\zeta}{\partial x}, \frac{\partial\zeta}{\partial y}\right) \quad [2.12]$$

is the two-dimensional gradient operator.

When the relationships [2.10] are satisfied, Eq. [2.5] reduces to

$$\nabla_{\mathrm{II}}^2\zeta = q^2\zeta. \quad [2.13]$$

By using Eq. [2.13] one obtains

$$(\nabla_{\parallel}\zeta)\cdot(\nabla_{\parallel}\zeta) = \nabla_{\parallel}\cdot(\zeta\nabla_{\parallel}\zeta) - \zeta\nabla_{\parallel}^2\zeta$$
$$= \nabla_{\parallel}\cdot(\zeta\nabla_{\parallel}\zeta) - q^2\zeta^2 \qquad [2.14]$$

Let V_m be the volume comprised between S_m and the meniscus surface $z = \zeta(x, y)$—see the hatched area in Fig. 1. Then

$$\int_{V_m} z dV = \int_{S_m} ds \int_0^{\zeta} z dz$$
$$= \frac{1}{2}\int_{S_m} \zeta^2 ds. \qquad [2.15]$$

From Eqs. [2.11], [2.14], and [2.15] one derives

$$\Delta A^P = I - q^2 \int_{V_m} z dV, \qquad [2.16]$$

where

$$I = \frac{1}{2}\int_{S_m} ds \nabla_{\parallel}\cdot(\zeta\nabla_{\parallel}\zeta). \qquad [2.17]$$

According to the Green theorem (see, e.g., Ref. (17))

$$I = \frac{1}{2}\sum_{K=1}^{N} \oint_{C_k} dl \boldsymbol{\mu}\cdot(\zeta\nabla_{\parallel}\zeta). \qquad [2.18]$$

The contours C_K and their orientation are shown in Fig. 2, where the unit running normal $\boldsymbol{\mu}$ is also depicted. The rectangle in Fig. 2 represents schematically the outer boundary of the region S_m, which is situated far away from the particles, where $\zeta\nabla_{\parallel}\zeta \to 0$. That is why the integral over it does not contribute to Eq. [2.18].

By substituting from Eqs. [2.6] and [2.16] into Eq. [2.8] one finally obtains

$$\Delta W_m = \gamma[I - I_\infty - \sum_{K=1}^{N}(A_K^c - A_{K\infty}^c)]$$
$$- \Delta\rho g\left(\int_{V_m} z dV - \int_{V_{m\infty}} z dV\right), \qquad [2.19]$$

where I is given by Eq. [2.18] and I_∞ is the limiting value of I for infinite interparticle separations. One can check that in view of Eqs. [2.2], [2.3], and [2.7] the integrals over V_m and $V_{m\infty}$ in the right-hand side of Eq. [2.19] cancel the integrals of $\zeta(x, y)$ arising from $Z_Y^{(c)}$. Thus Eq. [2.4] turns out to contain only integrals over the contact lines, particle surfaces, and volumes, but it does not contain integrals of the meniscus profile $\zeta(x, y)$. That is why simple analytical expressions for the capillary forces can be derived. This fact is illustrated below for two specified systems.

In conclusion it should be noted that the validity of Eq. [2.19] is restricted to meniscus surfaces of small slope, for which Eqs. [2.11] and [2.13] hold. As proven by Chan *et al.* (10) this restriction is always satisfied with small floating particles (small Bond number).

3. CAPILLARY INTERACTION BETWEEN TWO VERTICAL CYLINDERS

a. Energy of Capillary Interaction

Let us consider the capillary meniscus around two similar vertical circular cylinders, whose axes of symmetry are separated at a distance of $2s$. We will suppose that the contact angle α, subtended between the meniscus and cylinder surfaces (see Fig. 3), is close enough to 90° for Eqs. [2.10–2.19] to hold. In fact

$$\cos\alpha = -\boldsymbol{\mu}\cdot\mathbf{n}, \qquad [3.1]$$

where $\mathbf{n}$ is the unit normal to the meniscus surface at the contact line.

The geometry of the system suggests intro-

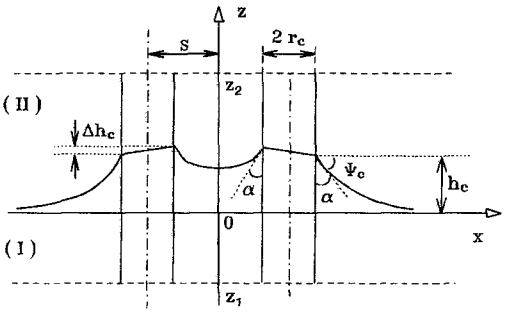

FIG. 3. Sketch of the capillary meniscus around two similar vertical cylinders of radius r_c; α is the contact angle, $2s$ is the distance between the axes of the cylinders.

duction of bipolar coordinates in the plane xy (see, e.g., Ref. (19)):

$$x = \frac{a \sinh \tau}{\cosh \tau - \cos \sigma}, \quad y = \frac{a \sin \sigma}{\cosh \tau - \cos \sigma}$$

$$-\pi \leqslant \sigma \leqslant \pi, \quad -\infty < \tau < +\infty. \quad [3.2]$$

Each line $\tau = \text{const}$ is a circumference (19)

$$(x - a \coth \tau)^2 + y^2 = \frac{a^2}{\sinh^2 \tau}, \quad [3.3]$$

see Fig. 4. If $\tau = \pm\tau_1$ is the equation of surfaces of the two cylinders, then in accordance with Eq. [3.3] and Fig. 3 one finds

$$r_c = a/\sinh \tau_1 \quad [3.4]$$

$$s = a \coth \tau_1. \quad [3.5]$$

From Eqs. [3.4–3.5] one derives

$$a = \sqrt{s^2 - r_c^2}. \quad [3.6]$$

The geometrical meaning of parameter a is illustrated in Fig. 4. If $\mathbf{e}_\tau$ is the running unit tangent to the τ lines, then Eq. [3.1] can be transformed to read

$$\cos \alpha = \mathbf{e}_\tau \cdot \mathbf{n}|_{\tau=\tau_1}. \quad [3.7]$$

By using the apparatus of differential geometry (see, e.g., Ref. (17)) one can derive

$$\mathbf{e}_\tau \cdot \mathbf{n}|_{\tau=\tau_1} = \frac{1}{\sqrt{g_{\tau\tau}}} \sqrt{\frac{g^*}{a_\zeta}} \frac{\partial \zeta}{\partial \tau}\bigg|_{\tau=\tau_1}. \quad [3.8]$$

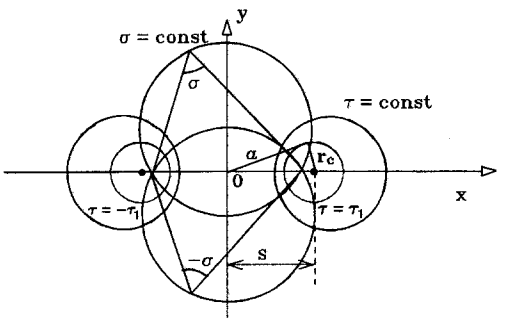

FIG. 4. Bicylindrical coordinates (σ, τ) in the plane xy. The two circumferences of radius r_c, corresponding to $\tau = \tau_1$, and $\tau = -\tau_1$, represent the contact line projections.

Here

$$g_{\tau\tau} = g_{\sigma\sigma} = \frac{a^2}{(\cosh \tau - \cos \sigma)^2} \quad [3.9]$$

are the components of the metric tensor of the space curvilinear coordinates $x = x(\sigma, \tau)$, $y = y(\sigma, \tau)$, $z = z$—cf. Eq. [3.2]. The determinant of this metric tensor is $g^* = g_{\sigma\sigma} g_{\tau\tau}$. Similarly a_ζ is the determinant of the surface metric tensor of the surface $z = \zeta(\sigma, \tau)$. One can derive that

$$a_\zeta = g_{\tau\tau} g_{\sigma\sigma} \left[1 + \frac{1}{g_{\sigma\sigma}} \left(\frac{\partial \zeta}{\partial \sigma}\right)^2\right] \times \left[1 + \frac{1}{g_{\tau\tau}} \left(\frac{\partial \zeta}{\partial \tau}\right)^2\right]. \quad [3.10]$$

In bipolar coordinates the relationships [2.10] read

$$\frac{1}{g_{\sigma\sigma}} \left(\frac{\partial \zeta}{\partial \sigma}\right)^2 \ll 1, \quad \frac{1}{g_{\tau\tau}} \left(\frac{\partial \zeta}{\partial \tau}\right)^2 \ll 1.$$

Then $a_\zeta \approx g_{\tau\tau} g_{\sigma\sigma}$, and the combination of Eqs. [3.7]–[3.9] yields

$$\sin \Psi_c \approx \frac{1}{\sqrt{g_{\tau\tau}}} \frac{\partial \zeta}{\partial \tau}\bigg|_{\tau=\tau_1} = \mathbf{e}_\tau \cdot \nabla_{II} \zeta|_{\tau=\tau_1}, \quad [3.11]$$

where

$$\sin \Psi_c = \cos \alpha, \quad [3.12]$$

see Fig. 3.

Since the cylinder radius, r_c, does not depend on s, then $A_K^c = A_{K\infty}^c$ $(K = 1, 2)$ and Eq. [2.19] reduces to

$$\Delta W_m = \gamma(I - I_\infty) - \Delta\rho g \left(\int_{V_m} z dV - \int_{V_{m\infty}} z dV\right). \quad [3.13]$$

Obviously for the contour C_1 $\mu = -\mathbf{e}_\tau$ (see Fig. 2) and from Eqs. [2.18] and [3.11] one obtains

$$I = \sin \Psi_c \oint_{C_1} dl\zeta. \quad [3.14]$$

It is taken into account in Eq. [3.14] that the integrals over the two circumferences C_1

and C_2 are equal—cf. Eq. [2.18]. At infinite distance between the cylinders from Eq. [3.14] one obtains

$$I_\infty = 2\pi r_c h_\infty \sin \Psi_c, \qquad [3.15]$$

where h_∞ is the elevation of the contact line over the plane xy at $s \to \infty$. In the case when $(qr_c)^2 \ll 1$ Derjaguin (20) has derived an expression for h_∞,

$$h_\infty = r_c \sin \Psi_c \ln \frac{4}{\gamma_e q r_c (1 + \cos \Psi_c)}, \qquad [3.16]$$

where $\gamma_e = 1.781072418 \cdots$ and $\ln \gamma_e$ is the number of Euler–Masceroni—see, e.g., Ref. (19), Section 21.4-1. The next term of the expansion of h_∞ for small $(qr_c)^2$ is derived in Refs. (21, 22).

In view of Eq. [2.2] and Fig. 3 for the system under consideration one derives

$$\sum_{K=1}^{2} \sum_{Y=I,II} \omega_{KY} A_{KY} = 4\pi r_c (z_2 \omega_{II} - z_1 \omega_I) + 2(\omega_I - \omega_{II}) \oint_{C_1} dl\zeta, \qquad [3.17]$$

where we have introduced the notation

$$\omega_{KY} \equiv \omega_Y, \quad K = 1, 2, \quad Y = I, II. \qquad [3.18]$$

Thus one obtains

$$\sum_{K=1}^{2} \sum_{Y=I,II} (\omega_{KY} A_{KY} - \lim_{s \to \infty} \omega_{KY} A_{KY}) = 2(\omega_I - \omega_{II}) \left(\oint_{C_1} dl\zeta - 2\pi r_c h_\infty \right). \qquad [3.19]$$

Besides, having in mind Eq. [2.3] one derives

$$\sum_{Y=I,II} m_Y g Z_Y^{(c)} = \sum_{Y=I,II} \rho_Y g \int_{V_Y} z dV = \frac{1}{2} g(\rho_{II} z_2^2 - \rho_I z_1^2) \int_{S_m} ds + \Delta\rho g \int_{V_m} z dV. \qquad [3.20]$$

Hence

$$\sum_{Y=I,II} [m_Y g Z_Y^{(c)} - \lim_{s \to \infty} m_Y g Z_Y^{(c)}] = \Delta\rho g \left[\int_{V_m} z dV - \int_{V_{m\infty}} z dV \right]. \qquad [3.21]$$

Finally, by using Eqs. [2.2], [2.7], [3.12–3.15], [3.19], and [3.21] one brings the expression [2.4] for the interaction energy in the form

$$\Delta W(s) = [2(\omega_I - \omega_{II}) + \gamma \sin \Psi_c] \times \left[\oint_{C_1} dl\zeta - 2\pi r_c h_\infty \right]. \qquad [3.22]$$

Note that when deriving Eq. [3.22] the volume integrals in the right-hand sides of Eq. [3.13] and [3.21] cancel each other.

In addition, if the contact angle α is the equilibrium one, i.e., if the Young equation,

$$\omega_{II} - \omega_I = \gamma \sin \Psi_c,$$

holds (cf. Eq. [3.12]), then Eq. [3.22] reduces to

$$\Delta W(s) = -2\pi\gamma r_c \sin \Psi_c (h_c - h_\infty), \qquad [3.23]$$

where by definition,

$$h_c = \frac{1}{2\pi r_c} \oint_{C_1} dl\zeta, \qquad [3.24]$$

h_c can be calculated by means of Eq. [3.54] derived below.

It will be shown below that $\Delta W(s)$ given by Eq. [3.23] is negative and corresponds to attraction between the two cylinders. It should also be noted that Eq. [3.23] holds for both positive and negative angles Ψ_c provided that the relationships [2.10] are satisfied.

b. Shape of the Meniscus around the Cylinders

Our aim below is to calculate the integral in the right-hand side of Eq. [3.24]:

$$\oint_{C_1} dl\zeta = \int_{-\pi}^{\pi} \zeta(\sigma, \tau_1) \frac{a d\sigma}{\cosh \tau_1 - \cos \sigma} \qquad [3.25]$$

($dl = \sqrt{g_{\sigma\sigma}}d\sigma$—see Eq. [3.9] and Ref. (17)). With this end in view we will first determine the shape of the meniscus around the cylinders.

In bipolar coordinates Eq. [2.13] has the form

$$(\cosh\tau - \cos\sigma)^2\left(\frac{\partial^2\zeta}{\partial\sigma^2} + \frac{\partial^2\zeta}{\partial\tau^2}\right) = (aq)^2\zeta(\sigma, \tau). \quad [3.26]$$

For liquid–gas and liquid–liquid interfaces q usually varies between 1 and 10 cm^{-1}. For $q = 10\ cm^{-1}$ and $a = 100\ \mu m$ one has $(aq)^2 = 10^{-2}$. Hence for $a \leqslant 100\ \mu m$ Eq. [3.26] contains a small parameter and the solution can be found in the form of an asymptotic expansion.

One sees that however small $(qa)^2$ may be, the right-hand side of Eq. [3.26] can be comparable with the left-hand side when σ and τ tend simultaneously to zero. That is why in connection with the method of the matched asymptotic expansions (see, e.g., Ref. (23)) we will consider an inner and an outer region:

inner region (close to the cylinders): $(\cosh\tau - \cos\sigma)^2 \gg (qa)^2$

outer region (far from the cylinders): $(\cosh\tau - \cos\sigma)^2 \leqslant (qa)^2$

In the inner region Eq. [3.26] reduces to

$$\frac{\partial^2\zeta}{\partial\sigma^2} + \frac{\partial^2\zeta}{\partial\tau^2} = 0. \quad [3.27]$$

(In fact, Eq. [3.27] determines the zeroth-order solution for ζ.) One can seek the solution of Eq. [3.27] in the form of a Fourier series:

$$\zeta(\sigma, \tau) = C_0 + B_0\tau + \sum_{n=1}^{\infty} B_n e^{-n\tau}\cos n\sigma, \quad \tau \geqslant 0. \quad [3.28]$$

The integration constants B_n, $n = 0, 1, 2 \ldots$, are to be determined from the boundary condition

$$\left.\frac{\partial\zeta}{\partial\tau}\right|_{\tau=\tau_1} = \frac{a\sin\Psi_c}{\cosh\tau_1 - \cos\sigma} \quad [3.29]$$

stemming from Eqs. [3.9] and [3.11]. By expanding the right-hand side of Eq. [3.29] into a Fourier series one obtains

$$\left.\frac{\partial\zeta}{\partial\tau}\right|_{\tau=\tau_1} = r_c\sin\Psi_c \times \left(1 + 2\sum_{n=1}^{\infty}\exp(-n\tau_1)\cos n\sigma\right), \quad [3.30]$$

where Eq. [3.4] is also taken into account. From Eqs. [3.28] and [3.30] one easily determines

$$B_0 = r_c\sin\Psi_c; \quad [3.31]$$

$$B_n = -\frac{2}{n}r_c\sin\Psi_c. \quad [3.32]$$

From Eqs. [3.28] and [3.31]–[3.32] one obtains the form of the solution for the whole region $-\infty < \tau < +\infty$,

$$\zeta(\sigma, \tau) = C_0 + r_c\sin\Psi_c\ln(2\cosh\tau - 2\cos\sigma), \quad [3.33]$$

where we have used the identity

$$|\tau| - 2\sum_{n=1}^{\infty}\frac{1}{n}\exp(-n|\tau|)\cos\sigma = \ln(2\cosh\tau - 2\cos\sigma). \quad [3.34]$$

Along the outer part of x axis ($\sigma = 0$) Eq. [3.33] yields

$$\zeta(0, \tau) = C_0 + r_c\sin\Psi_c \times [\tau + 2\ln(1 - e^{-\tau})], \quad \tau > 0. \quad [3.35]$$

For large x by using the expression for $\tau(x, y)$ in Ref. (19) one obtains

$$\tau|_{y=0} = \ln\left|\frac{x + a}{x - a}\right| = 2\left[\frac{a}{x} + 0(a^3/x^3)\right]. \quad [3.36]$$

Then from Eqs. [3.35]–[3.36] one derives

$$\zeta(0, \tau) = C_0 + r_c\sin\Psi_c \times \left[2\ln\frac{2a}{x} + 0(a^2/x^2)\right], \quad x \gg 1. \quad [3.37]$$

On the other hand, along the y axis ($\tau = 0$) Eq. [3.33] reduces to

$$\zeta(\sigma, 0) = C_0 + r_c \sin \Psi_c \ln\left(4 \sin^2 \frac{\sigma}{2}\right). \quad [3.38]$$

In addition, for $\tau = 0$ Eq. [3.2] yields

$$\sin^2 \frac{\sigma}{2} = (1 + y^2/a^2)^{-1}. \quad [3.39]$$

Then the asymptotics of the inner solution $\zeta(\sigma, \tau)$, Eq. [3.33], along the y axis reads

$$\zeta(\sigma, 0) = C_0 + r_c \sin \Psi_c \times \left[2 \ln \frac{2a}{y} + 0(a^2/y^2)\right], \quad y \gg 1. \quad [3.40]$$

The comparison between Eqs. [3.37] and [3.40] shows that the *outer* asymptotics of the *inner* solution is axisymmetrical, i.e., one can write

$$(\zeta^{in})^{out} = C_0 + r_c \sin \Psi_c \left[2 \ln \frac{2a}{r} + 0(a^2/r^2)\right], \quad [3.41]$$

where

$$r = \sqrt{x^2 + y^2}. \quad [3.42]$$

The above result implies that the meniscus surface in the outer region ($\sigma \ll 1$, $\tau \ll 1$) is axisymmetrical. Hence in the outer region Eq. [2.13] reduces to

$$\frac{1}{r} \frac{d}{dr}\left(r \frac{d\zeta}{dr}\right) = q^2 \zeta. \quad [3.43]$$

Along with the outer boundary condition

$$\lim_{r \to \infty} \zeta(r) = 0, \quad [3.44]$$

Eq. [3.43] yields

$$\zeta^{out}(r) = GK_0(qr), \quad [3.45]$$

where G is an integration constant and K_0 is modified Bessel function—see, e.g., (19, 24). The constant G as well as the constant C_0 in Eq. [3.33] is to be determined by means of the condition of matching of the outer and inner solutions (see Ref. (23)):

$$(\zeta^{in})^{out} = (\zeta^{out})^{in}. \quad [3.46]$$

By expanding the right-hand side of Eq. [3.45] in series for small qr one obtains

$$(\zeta^{out})^{in} = G[-\ln(\gamma_e qr/2) + 0(q^2 r^2)]. \quad [3.47]$$

By substitution from Eqs. [3.41] and [3.47] into Eq. [3.46] one determines

$$G = 2r_c \sin \Psi_c,$$

$$C_0 = -2r_c \sin \Psi_c \ln(\gamma_e qa). \quad [3.48]$$

Hence the inner solution [3.33] and the outer solution [3.45] acquire the form

$$\zeta^{in}(\sigma, \tau) = r_c \sin \Psi_c[-2 \ln(\gamma_e qa) + \ln(2 \cosh \tau - 2 \cos \sigma)] \quad [3.49]$$

$$\zeta^{out}(r) = 2r_c \sin \Psi_c K_0(qr). \quad [3.50]$$

Then the solution, which is uniformly valid in the inner and outer region is (23):

$$\zeta = \zeta^{in} + \zeta^{out} - (\zeta^{out})^{in}, \quad [3.51]$$

where in view of Eqs. [3.47]–[3.48]

$$(\zeta^{out})^{in} = -2r_c \sin \Psi_c \ln(\gamma_e qr/2). \quad [3.52]$$

In accordance with Eqs. [3.24]–[3.25] the mean elevation h_c of the contact line over the plane xy is

$$h_c = \frac{a}{2\pi r_c} \int_{-\pi}^{\pi} \zeta^{in}(\sigma, \tau_1) \frac{d\sigma}{\cosh \tau_1 - \cos \sigma}. \quad [3.53]$$

The substitution from Eq. [3.49] into Eq. [3.53] yields

$$h_c = r_c \sin \Psi_c \times \left[\tau_1 + 2 \ln \frac{1 - \exp(-2\tau_1)}{\gamma_e qa}\right]. \quad [3.54]$$

From Eq. [3.4] it follows that

$$\tau_1 = \ln(a/r_c + \sqrt{1 + a^2/r_c^2}). \quad [3.55]$$

Equations [3.54]–[3.55] provide the sought-

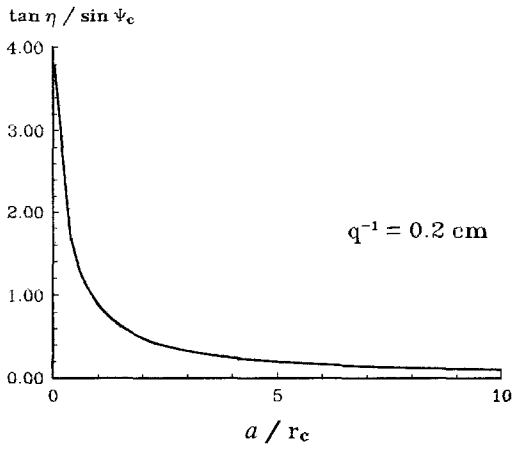

FIG. 5. Plot of $\tan \eta/\sin \Psi_c$ vs a/r_c.

for dependence of h_c on a, which in combination with Eq. [3.23] gives the capillary interaction energy ΔW as a function of distance s between the two cylinders—cf. Eq. [3.5].

It should be noted that Eq. [3.54] is valid when

$$(qa)^2 \ll 1, \quad \sin^2\Psi_c \ll 1. \qquad [3.56]$$

Hence a boundary transition $a \to \infty$ (infinite distance between the cylinders) in Eq. [3.54] does not make sense. In the other limit, $a \to 0$, from [3.54]–[3.55] one obtains the maximum value of h_c,

$$h_c(a \to 0) = 2r_c \sin \Psi_c \ln \frac{2}{\gamma_e q r_c} \approx 2h_\infty, \qquad [3.57]$$

cf. Eqs. [3.16] and [3.56].

Equation [3.49] shows that at fixed $\tau = \tau_1$, ζ^{in} depends on σ, i.e., the contact line is not horizontal. The slope of the contact line can be characterized by the angle η defined as follows:

$$\tan \eta = [\zeta^{in}(\pi, \tau_1) - \zeta^{in}(0, \tau_1)]/(2r_c) \qquad [3.58]$$

By means of Eq. [3.49] one obtains

$$\tan \eta = \sin \Psi_c \ln \frac{1 + \exp(-\tau_1)}{1 - \exp(-\tau_1)}. \qquad [3.59]$$

The plot of $(\tan \eta)/\sin \Psi_c$ vs a/r_c is shown in Fig. 5. One sees that for $a/r_c > 3$ the inclination of the contact line is very small ($\tan \eta < 0.1$) even if $\Psi_c = 20°$.

4. CAPILLARY INTERACTION BETWEEN TWO SPHERES

Let us consider a flat horizontal plate covered with a liquid layer of thickness l_0 (Phase I). In addition, let us consider two similar spheres of radius R, which are put on the plate. If $2R > l_0$ the spheres protrude from Phase I and lines of three-phase contact are formed—see Fig. 6. We again restrict our considerations to the case of small slope of the meniscus surface ($\sin^2\Psi_c \ll 1$—see Fig. 6) and to small inclination of the contact line from horizontal position. In this case the horizontal projection of the contact line can be treated approximately as a circumference of radius r_c. In addition, Eqs. [3.11] and [3.14] hold again. However, instead of Eq. [3.12] in the present case one is to write

$$\Psi_c + \alpha = \arcsin(r_c/R), \qquad [4.1]$$

where α is the real contact angle—cf. Fig. 6. Besides, Eq. [3.15] is to be written in the form

$$I_\infty = 2\pi r_\infty h_\infty \sin \Psi_\infty, \qquad [4.2]$$

where r_∞ and Ψ_∞ are the limiting values of r_c and Ψ_c for $s \to \infty$. In this way Eq. [2.19] takes the form

$$\Delta W_m = 2\pi\gamma[r_c h_c \sin \Psi_c - r_\infty h_\infty \sin \Psi_\infty - r_c^2 + r_\infty^2] - \Delta\rho g\left(\int_{V_m} z dV - \int_{V_{m\infty}} z dV\right), \qquad [4.3]$$

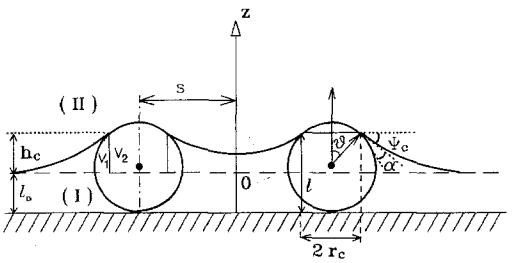

FIG. 6. Sketch of two spheres of radius R partially immersed in a liquid layer of thickness l_0 on a horizontal substrate.

where h_c is defined by Eq. [3.24]. The counterpart of Eq. [3.19] for the present case reads

$$\sum_{K=1}^{2}\sum_{Y=\mathrm{I,II}}(\omega_{KY}A_{KY}-\lim_{s\to\infty}\omega_{KY}A_{KY}) = 4\pi R(\omega_{\mathrm{I}}-\omega_{\mathrm{II}})(h_c-h_\infty). \quad [4.4]$$

By means of some geometrical considerations one can derive

$$\int_{V_{\mathrm{I}}} zdV-\int_{V_{\mathrm{I}\infty}} zdV=\int_{V_m} zdV - \int_{V_{m\infty}} zdV-2\left[\int_{V_1} zdV-\int_{V_{1\infty}} zdV\right] \quad [4.5]$$

$$\int_{V_{\mathrm{II}}} zdV-\int_{V_{\mathrm{II}\infty}} zdV=-\int_{V_m} zdV + \int_{V_{m\infty}} zdV-2\left[\int_{V_2} zdV-\int_{V_{2\infty}} zdV\right]. \quad [4.6]$$

The volumes V_1 and V_2 represent part of the particle volume and are shown in Fig. 6. The boundary between them is a part of a cylindrical surface based on the contact line. One can easily derive that

$$\int_{V_1} zdV-\int_{V_{1\infty}} zdV=\pi\int_{h_\infty}^{h_c} dzzr_s^2(z) - \frac{\pi}{2}(r_c^2h_c^2-r_\infty^2h_\infty^2) = -\left[\int_{V_2} zdV-\int_{V_{2\infty}} zdV\right], \quad [4.7]$$

where

$$r_s^2(z)=R^2-(z-R+l_0)^2 \quad [4.8]$$

is the equation of the spherical particle surface. Then by making use of Eqs. [4.5]–[4.8] one obtains a counterpart of Eq. [3.21],

$$\sum_{Y=\mathrm{I,I}}(m_Ygz_Y^{(c)}-\lim_{s\to\infty}m_Ygz_Y^{(c)}) = \Delta\rho g\left[\int_{V_m} zdV-\int_{V_{m\infty}} zdV - 2\left(\int_{V_1} zdV-\int_{V_{1\infty}} zdV\right)\right], \quad [4.9]$$

where as usual $\Delta\rho=\rho_{\mathrm{I}}-\rho_{\mathrm{II}}$. Finally, a substitution from Eqs. [2.2], [2.7], [4.3], [4.4], and [4.9] into Eq. [2.4] leads to the following expression for the interaction energy between the two particles

$$\Delta W(s)=4\pi R(\omega_{\mathrm{I}}-\omega_{\mathrm{II}})(h_c-h_\infty) - 2\pi\gamma(-r_ch_c\sin\Psi_c+r_c^2 + r_\infty h_\infty\sin\Psi_\infty-r_\infty^2) - 2\Delta\rho g\left(\int_{V_1} zdV-\int_{V_{1\infty}} zdV\right). \quad [4.10]$$

If the Young equation $\omega_{\mathrm{II}}-\omega_{\mathrm{I}}=\gamma\cos\alpha$ is satisfied (equilibrium contact line without contact angle hysteresis), Eq. [4.10] transforms to read

$$\Delta W(s)=-2\pi\gamma[2(h_c-h_\infty)R\cos\alpha - r_ch_c\sin\Psi_c+r_c^2+r_\infty h_\infty\sin\Psi_\infty-r_\infty^2] - 2\Delta\rho g\left(\int_{V_1} zdV-\int_{V_{1\infty}} zdV\right). \quad [4.11]$$

By means of [4.7]–[4.8] one easily calculates

$$\int_{V_1} zdV-\int_{V_{1\infty}} zdV=\frac{\pi}{2}\left\{\frac{1}{2}(h_c^2-h_\infty^2) \times[2l_0(2R-l_0)-h_c^2-h_\infty^2] + \frac{4}{3}(R-l_0)(h_c^3-h_\infty^3) - r_c^2h_c^2+r_\infty^2h_\infty^2\right\}. \quad [4.12]$$

The numerical calculations show, that usually the last term in Eq. [4.11] turns out to be negligible. Eqs. [4.11]–[4.12] in conjunction with Eq. [3.54] for h_c and the Derjaguin (20) formula,

$$h_\infty=r_\infty\sin\Psi_\infty\ln\frac{2}{\gamma_e q r_\infty}, \quad [4.13]$$

allow calculation of the capillary interaction energy ΔW between the two spherical particles. The corresponding capillary force is

$$f=-\frac{d(\Delta W)}{d(2s)}. \quad [4.14]$$

Numerical results for the capillary interactions are given in the next section.

5. NUMERICAL RESULTS AND DISCUSSION

The capillary interactions between particles attached to a liquid–fluid interface are important in a very wide region of particle size: from 10^{-7} cm up to 10^{-1} cm. The interest of the experimentalists is increased to the region of the micrometer-size particles (e.g., polystyrene latexes—see Refs. (4, 5)) and to the region around 10 nm (macromolecular globules—see Refs. (6–8)). That is why in the illustrative numerical study below we will focus our attention on particle size of the order of 10 nm and 1 μm. Of course, the theoretical expressions derived in the previous sections have a wider range of validity.

a. Capillary Interaction between Two Vertical Cylinders

First of all we consider the dependence of the contact line elevation h_c on the distance between the cylinders for a given angle Ψ_c. The calculative procedure is the following. For a given s and cylinder radius r_c from Eq. [3.6] one determines a—see also Fig. 4. Then one calculates τ_1 from Eq. [3.55] and h_c from Eq. [3.54]. h_∞ is given by Eq. [3.16]. Figure 7 represents the ratio h_c/h_∞ as a function of a/r_c for two different values of r_c: 6 nm and 800 nm. As could be expected, h_c decreases when the distance between cylinders increases. The curves in Fig. 7 are insensitive to the value of Ψ_c (if only $|\Psi_c| \leqslant 20°$ in order for Eq. [3.56] to hold). It is worthwhile noting that the two curves in Fig. 7 do not differ too much in spite of the great difference between the values of r_c.

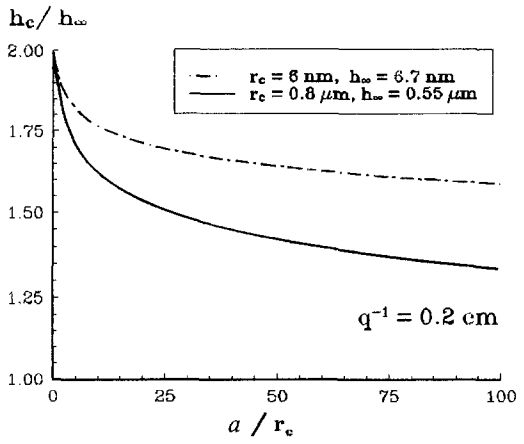

FIG. 7. Plot of h_c/h_∞ vs a/r_c for cylinders.

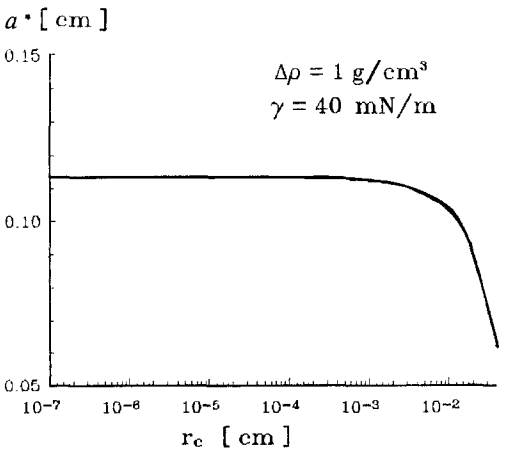

FIG. 8. The radius of validity of Eq. [3.54] a^* as a function of the cylinder radius r_c.

As mentioned earlier, Eq. [3.54] for h_c is valid when $(qa)^2 \ll 1$. For sufficiently large values of a the values of h_c calculated by means of Eq. [3.54] are not correct, e.g., the ratio h_c/h_∞ depicted in Fig. 7 can be less than unity and even negative. Let $a = a^*$ be the solution of the equation $h_c(a) = h_\infty$. For $a > a^*$ Eq. [3.54] is no more valid ($h_c < h_\infty$). Hence a^* provides an estimate of the boundary of validity of Eq. [3.54]. Figure 8 represents a^* vs r_c calculated by means of Eq. [3.16] and [3.54]–[3.55]. To determine q we used γ = 40 mN/m and $\Delta\rho$ = 1 g/cm^3—see Eq. [2.6]. The region of validity of Eq. [3.54] corresponds to $a < a^*$. It is remarkable that for $r_c < 100$ μm a^* is constant and equal to $(\gamma_e q)^{-1}$. For $r_c > 100$ μm a^* (and the range of validity of Eq. [3.54]) decreases fast.

Having calculated h_c and h_∞ one can easily determine the energy of capillary interaction ΔW by means of Eq. [3.23]. The plot of ΔW

vs a/r_c is presented in Fig. 9 for various values of r_c and Ψ_c. One sees that ΔW is negative and corresponds to attraction between the two cylinders. Since ΔW is an even function of Ψ_c (cf. Eqs. [3.16], [3.23], and [3.54]), ΔW is negative for both concave and convex menisci ($\Psi_c > 0$ or $\Psi_c < 0$). Besides, the magnitude of ΔW increases with r_c proportionally to r_c^2 and with Ψ_c proportionally to $\sin^2\Psi_c$.

Another feature of the capillary force interaction energy is that ΔW is extremely long-ranged—see Fig. 9. This fact implies that in the case of more than two cylinders the capillary interaction will not be pair-wise additive and many-body interactions must be taken into account.

b. Single Sphere Protruding from a Liquid Layer

To calculate parameters r_∞, Ψ_∞, and h_∞ entering Eq. [4.11] we used the following procedure. We suppose that the sphere radius R, the layer thickness l_0, and the contact angle α (see Fig. 6) are known. Let us define

$$l_\infty = l_0 + h_\infty. \qquad [5.1]$$

In the case of consideration, when a three-phase contact line is formed, one has $l_0 < l_\infty < 2R$. If l_∞ is known, from the equation of sphere one finds

$$r_\infty(l_\infty) = [l_\infty(2R - l_\infty)]^{1/2}. \qquad [5.2]$$

Then from Eq. [4.1] one determines

$$\Psi_\infty(l_\infty) = \arcsin\frac{r_\infty(l_\infty)}{R} - \alpha. \qquad [5.3]$$

Finally, a combination of Eqs. [3.16] (with $\Psi_c = \Psi_\infty$) and [5.1] yields

$$l_\infty = l_0 - r_\infty(l_\infty)\sin\Psi_\infty(l_\infty) \times \ln[\gamma_e q r_\infty(l_\infty)(1 + \cos\Psi_\infty(l_\infty))/4]. \qquad [5.4]$$

In view of Eqs. [5.2]–[5.3], Eq. [5.4] represents an equation for calculating l_∞, which is to be solved numerically. Figures 10a and 10b show the dependences of Ψ_∞ and h_∞ on l_0 for contact angle $\alpha = 0$ and for two values of the particle radius R. Striking facts are that even for $l_0 \to 0$ the particle is encircled by a thick meniscus and that Ψ_c can not exceed 30° for the values of R considered. It should be also noted that for the smaller particle ($R = 6$ nm) disjoining pressure effects, which are not accounted for in Eq. [5.4], can be important—see, e.g., (25). This is discussed by the end of the next subsection.

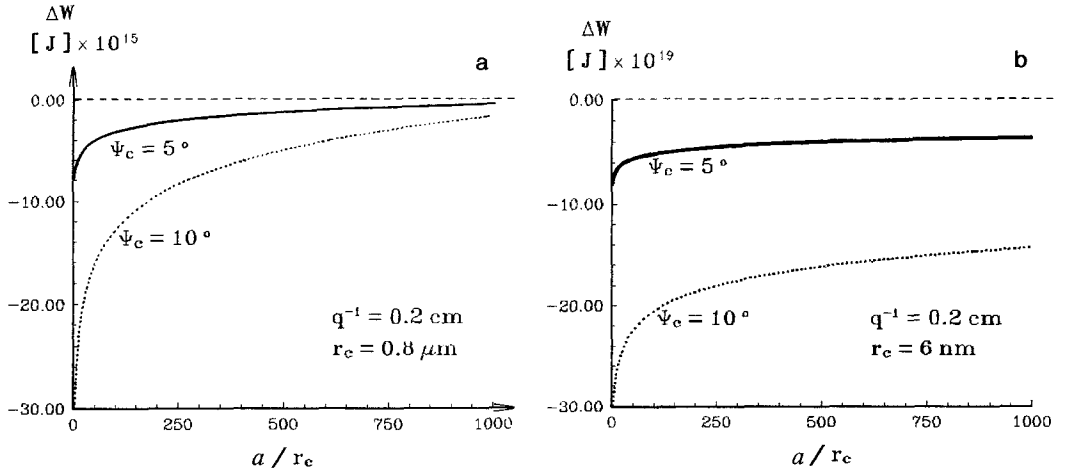

FIG. 9. Capillary meniscus interaction energy ΔW vs the distance between two vertical cylinders characterized by a/r_c with r_c being the cylinder radius.

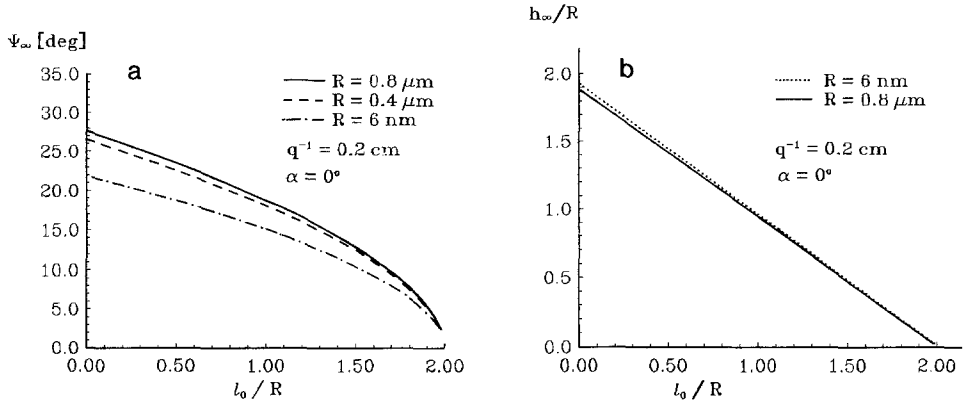

FIG. 10. Angle of meniscus slope Ψ_c (a) and elevation of the contact line h_c (b) vs the liquid layer thickness l_0 for a single partially immersed sphere of radius R.

c. *Two Spheres Protruding from a Liquid Layer*

In the case of two spheres of the same radius R instead of Eq. [5.4] one has

$$l = l_0 + h_c[r_c(l), \Psi_c(l), a(l)], \quad [5.5]$$

where h_c is given by Eqs. [3.54]–[3.55] along with the expressions

$$r_c(l) = [l(2R - l)]^{1/2},$$

$$\Psi_c(l) = \arcsin \frac{r_c(l)}{R} - \alpha \quad [5.6]$$

$$a(l) = [s^2 - r_c^2(l)]^{1/2}. \quad [5.7]$$

To determine l we solved Eq. [5.5] numerically. The results for h_c/h_∞ vs s/R are shown in Fig. 11. One sees from Figs. 10b and 11 that both h_∞ and the ratio h_c/h_∞ increase when the thickness of the liquid layer l_0 decreases. Besides, h_c increases when the distance $2s$ between particle centers at a given thickness l_0 decreases.

By using the values of $r_c(l)$, $\Psi_c(l)$, and $a(l)$ determined as explained above one can estimate the deviation of the contact line from horizontal position by means of Eqs. [3.55] and [3.59]. The calculated $\tan \eta / \sin \Psi_c$ is plotted in Fig. 12 vs a/R. One sees that for micrometer size particles the inclination of the contact line is negligible. This fact supports our assumption that the contours C_1 and C_2 depicted in Fig. 2 are circumferences in the case of small spherical particles.

Figure 13 represents the dependence of the capillary interaction free energy ΔW on the distance between particles for particle radius $R = 0.8$ μm and contact angle $\alpha = 0°$. ΔW was determined by means of Eq. [4.11] along with the values of the geometrical parameters calculated from Eqs. [5.2]–[5.7]. The most important fact is that ΔW is negative and corresponds to attraction between the particles. Besides, the capillary interaction turns out to

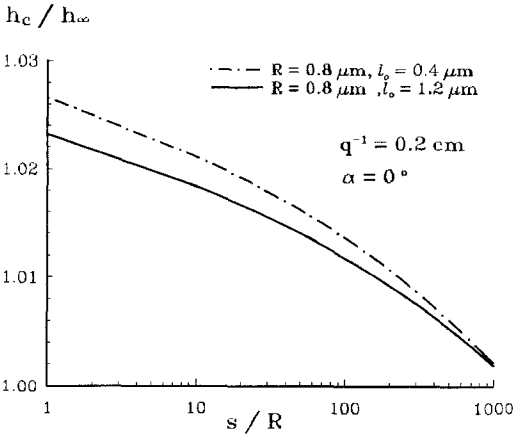

FIG. 11. Plot of h_c/h_∞ vs s/R where $2s$ is the center-to-center separation between two similar spheres of radius R.

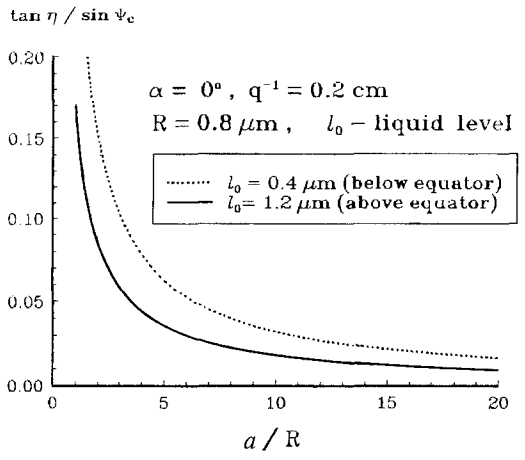

FIG. 12. Plot of $\tan \eta / \sin \Psi_c$ vs a/R; η characterizes the deviation of the contact line from horizontal position—see Eq. [3.58].

be long-ranged: even at $s = 1000R$, $|\Delta W|$ is considerably larger than the thermal energy k_BT. Such a long-range attraction could lead to two-dimensional disorder–order phase transitions and formation of ordered clusters or larger domains of particles depending on their concentration as observed in Ref. (26). As seen in Fig. 13 the attraction increases when the thickness l_0 of the liquid layer around the particles decreases. This effect is illustrated also in Fig. 14 for different values of the contact angle at fixed interparticle distance $2s = 5R$. The attraction is larger for small thickness l_0 and small contact angle α. When $l_0 = R(1 + \cos \alpha)$ both angle Ψ_c and the meniscus elevation h_c are equal to zero at every interparticle separation. For this l_0 one obtains $\Delta W = 0$ and the curves in Fig. 14 exhibit a maximum. The points on the right from the maximum correspond to negative Ψ_c and h_c (the contact line is situated below the level of the horizontal interface far from the particles). It is worthwhile to note that in spite of the large variation of α for the curves in Fig. 14, the slope angles Ψ_c and Ψ_∞ determined from Eqs. [5.2]–[5.7] turn out to be small enough to satisfy Eq. [3.56].

The approach for the calculation of ΔW for two similar spheres or cylinders developed in this study can be extended for the case of cylinders and/or spheres of different radii and contact angles. Such a study is under way (27).

When the particles are small (e.g., macromolecular globules—see Refs. (6–8)) and the liquid layer shown in Fig. 6 is thin, the effect of the *disjoining pressure* should be taken into account. The disjoining pressure enters the Laplace equation and hence it affects the me-

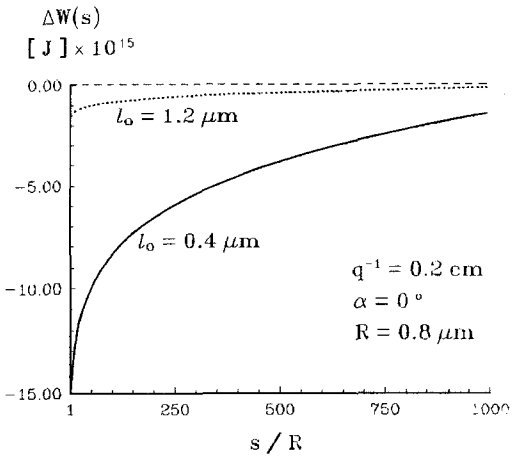

FIG. 13. Dependence of the capillary meniscus interaction energy ΔW on the distance $2s$ between the centers of two similar spheres of radius R for two values of the liquid layer thickness l_0.

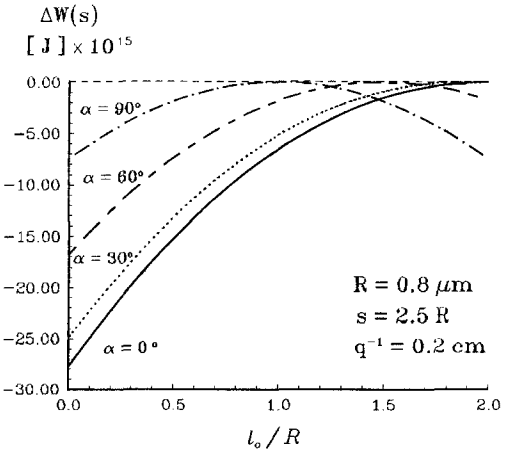

FIG. 14. Plot of ΔW vs l_0/R for different values of the contact angle α at fixed distance $2s = 5R$ between the centers of two similar spheres of radius R.

niscus shape. For small meniscus slope (cf. Eq. [2.10]) from Eq. [5] in Ref. (25) or from Eq. [4.11] in Ref. (28) one can derive

$$\gamma\nabla^2\zeta = P_c - \Pi, \qquad [5.8]$$

where P_c and Π are the capillary and disjoining pressures, respectively. The capillary pressure can be represented in the form

$$P_c = P_{II}^{(0)} - P_I^{(0)} + \Delta\rho g\zeta, \qquad [5.9]$$

where $P_Y^{(0)}$, $Y = I, II$, is the hydrostatic pressure in the respective phase at level $z = 0$—see Fig. 6. It is natural to suppose that the film of thickness $h = l_0$ is an equilibrium wetting film. Then the disjoining pressure can be expanded in series for small ζ:

$$\Pi = P_{II}^{(0)} - P_I^{(0)} + \left(\frac{d\Pi}{dh}\right)\Big|_{\zeta=0}\zeta + \cdots. \qquad [5.10]$$

(For $\zeta = 0$ Eqs. [5.9]–[5.10] yield $\Pi = P_c$ as it should be for an equilibrium flat film—see, e.g., Ref. (29).) The substitution from Eqs. [5.9]–[5.10] into Eq. [5.8] leads to

$$\nabla_{II}^2\zeta = \tilde{q}^2\zeta \qquad [5.11]$$

where

$$\tilde{q}^2 = \frac{\Delta\rho g}{\gamma} - \frac{\Pi'}{\gamma}, \quad \Pi' = \frac{d\Pi}{dh}\Big|_{\zeta=0}. \qquad [5.12]$$

For equilibrium films $\Pi' < 0$ and hence $\tilde{q}^2$ is a positive quantity. The comparison between Eqs. [5.11] and [2.13] reveals that the disjoining pressure effect can be accounted for by changing formally q to $\tilde{q}$ in Eqs. [3.49]–[3.52], [3.54], and [4.13] describing the meniscus profile. The contribution of Π into the capillary interaction energy ΔW needs a special study, which is outside the scope of the present paper.

Equation [5.12] shows that the disjoining pressure effect becomes important when

$$-\Pi'(h) \geqslant \Delta\rho g. \qquad [5.13]$$

As an illustration let us consider the simplest disjoining pressure isotherm, that of the van der Waals forces,

$$\Pi(h) = -\frac{A_H}{6\pi h^3}, \qquad [5.14]$$

where A_H is the compound Hamaker constant—see, e.g., Ref. (30). From Eqs. [5.13]–[5.14] one can conclude that the disjoining pressure becomes important when the film thickness h satisfies the relationship

$$h \leqslant (-A_H/2\pi\Delta\rho g)^{1/4}. \qquad [5.15]$$

For an aqueous film on mercury, like those studied in Refs. (6, 7), one has $A_H = -7.22 \times 10^{-20}$ J (van der Waals repulsion)—see Ref. (31). With this value of A_H Eq. [5.15] yields $h \leqslant 1.0$ μm. The latter value is somewhat exaggerated for the reason that Eq. [5.14] is not valid for such large thickness because of the electromagnetic retardation effect—cf. Ref. (30).

CONCLUDING REMARKS

A general expression for the energy of capillary interaction between particles attached to a liquid–fluid interface is proposed—see Eqs. [2.2] and [2.4]. The weight of the particles and of the capillary menisci around them as well as the surface energy of all phase boundaries are taken into account. In the case of small slope of the meniscus surface, when the Laplace equation can be linearized, all integrals over the *meniscus* surface and volume (the volume hatched in Fig. 1) cancel each other. Then it turns out, that the capillary interaction energy ΔW is expressed only through integrals over the *particle* surface and volume, and over the lines of three-phase contact.

In the case of two vertical cylinders the general equations lead to a simple expression for ΔW, Eq. [3.23]. ΔW depends on the elevation, h_c, of the contact line over the horizontal interface far from the cylinders. To derive an expression for h_c we solved the Laplace equation in the case, when $(qa)^2$ is a small parameter (cf. Eq. [2.6] and Fig. 4). The method of the matched asymptotic expansions is used.

Eqs. [3.49], [3.50], and [3.51] represent the inner, the outer, and the uniformly valid solution, respectively. Equation [3.54] gives the sought-for expression for the elevation h_c.

The general equations are applied also to calculate the energy of capillary interaction between two similar spheres protruding from a horizontal liquid layer—see Fig. 6 and Eq. [4.11]. Both for spheres and cylinders the energy of capillary interaction turns out to be attractive and long-ranged—see Figs. 9a and 9b as well as 13a and 13b. Hence the capillary forces should be taken into account when interpreting experimental data for particle ordering at an interface—see, e.g., (4–7).

The present study can find a further development in several aspects: (i) The capillary interactions between *two particles* under other geometrical configurations can be investigated. (ii) When the particle-containing layer is thin, the effect of *disjoining pressure* on the meniscus profile should also be taken into account—see Eq. [5.13].

We hope the present study will contribute to a better understanding of phenomena like cluster formation and particle ordering at a liquid–fluid interface.

ACKNOWLEDGMENTS

This study was financially supported by the Research and Development Corporation of Japan under the Nagayama Protein Array Project of ERATO Program. The authors are indebted to Mrs. R. Alargova for drawing the figures.

REFERENCES

1. Gerson, D. F., Zaijc, J. E., and Ouchi, M. D., *in* "Chemistry for Energy" (M. Tomlinson, Ed.), ACS Symp. Series, Vol. 90, p. 66. Amer. Chem. Soc., Washington DC, 1979.
2. Henry, J. D., Prudich, M. E., and Vaidyanathan, K. R., *Sep. Purif. Methods* **8,** 81 (1979).
3. Hinsch, K., *J. Colloid Interface Sci.* **92,** 243 (1983).
4. Pieranski, P., *Phys. Rev. Lett.* **45,** 569 (1980).
5. Onoda, G. Y., *Phys. Rev. Lett.* **55,** 226 (1985).
6. Yoshimura, H., Endo, S., Matsumoto, M., Nagayama, K., and Kagawa, Y., *J. Biochem.* **106,** 958 (1989).
7. Yoshimura, H., Matsumoto, M., Endo, S., and Nagayama, K., *Ultramicroscopy* **32,** 265 (1990).
8. Haggerty, L., Watson, B. A., Barteau, M. A., and Lenhoff, A. M., *J. Vac. Sci. Technol.* **B9,** 1219 (1991).
9. Nicolson, M. M., *Proc. Cambridge Philos. Soc.* **45,** 288 (1949).
10. Chan, D. Y. C., Henry, J. D., and White, L. R., *J. Colloid Interface Sci.* **79,** 410 (1981).
11. Gifford, W. A., and Scriven, L. E., *Chem. Eng. Sci.* **26,** 287 (1971).
12. Fortes, M. A., *Can. J. Chem.* **60,** 2889 (1982).
13. Benson, G. C., and Yun, K. S., *in* "The Solid-Gas Interface" (E. A. Flood, Ed.), Vol. 1, p. 203. Dekker, New York, 1967.
14. Gurkov, T. D., and Kralchevsky, P. A., *Colloids Surf.* **47,** 45 (1990).
15. Princen, H. M., *in* "Surface and Colloid Science" (E. Matijević and F. R. Eirich, Eds.), Vol. 2, p. 1. Wiley, New York, 1969.
16. Finn, R., "Equilibrium Capillary Surfaces." Springer-Verlag, New York, 1986.
17. McConnell, A. J., "Application of Tensor Analysis." Dover, New York, 1957.
18. Ivanov, I. B., Kralchevsky, P. A., and Nikolov, A. D., *J. Colloid Interface Sci.* **112,** 97 (1986).
19. Korn, G. A., and Korn, T. M., "Mathematical Handbook." McGraw-Hill, New York, 1968.
20. Derjaguin, B., *Dokl. Akad. Nauk USSR* **51,** 517 (1946).
21. Lo, L. L., *J. Fluid Mech.* **132,** 65 (1983).
22. Kralchevsky, P. A., Ivanov, I. B., and Nikolov, A. D., *J. Colloid Interface Sci.* **112,** 108 (1986).
23. Nayfeh, A. H., "Perturbation Methods." Wiley, New York, 1973.
24. Abramovitz, M., and Stegun, I. A., "Handbook of Mathematical Functions." Dover, New York, 1965.
25. Kralchevsky, P. A., and Ivanov, I. B., *Chem. Phys. Lett.* **121,** 116 (1985).
26. Denkov, N. D., Velev, O. D., Kralchevsky, P. A., Ivanov, I. B., Yoshimura, H., and Nagayama, K., *Nature,* submitted for publication.
27. Kralchevsky, P. A., Paunov, V. N., Denkov, N. D., Ivanov, I. B., and Nagayama, K., *J. Colloid Interface Sci.,* submitted for publication.
28. Kralchevsky, P. A., and Ivanov, I. B., *J. Colloid Interface Sci.* **137,** 234 (1990).
29. Toshev, B. V., and Ivanov, I. B., *Colloid Polym. Sci.* **253,** 558 (1975).
30. Nir, S., and Vassilieff, C. S., *in* "Thin Liquid Films" (I. B. Ivanov, Ed.), p. 207. Dekker, New York, 1988.
31. Usui, S., Sasaki, S., and Hasegawa, F., *Colloids Surf.* **18,** 53 (1986).